Population distribution of wavefront aberrations in the peripheral human eye

Linda Lundström,[1,2,*] Jörgen Gustafsson,[3] and Peter Unsbo[2]

[1]*Laboratorio de Optica, Universidad de Murcia, 300 71 Murcia, Spain*
[2]*Biomedical and X-ray Physics, Royal Institute of Technology, 106 91 Stockholm, Sweden*
[3]*School of Optometry, University of Kalmar, 391 82 Kalmar, Sweden*
**Corresponding author: linda@biox.kth.se*

Received May 8, 2009; revised August 7, 2009; accepted August 12, 2009;
posted August 13, 2009 (Doc. ID 110590); published September 16, 2009

We present a population study of peripheral wavefront aberrations in large off-axis angles in terms of Zernike coefficients. A laboratory Hartmann–Shack sensor was used to assess the aberrations in 0°, 20°, and 30° in the nasal visual field of 43 normal eyes. The elliptical pupil meant that the quantification could be done in different ways. The three approaches used were (1) over a circular aperture encircling the pupil, (2) over a stretched version of the elliptical pupil, and (3) over a circular aperture within the pupil (MATLAB conversion code given). Astigmatism (c_2^2) increased quadratically and coma (c_3^1) linearly with the horizontal viewing angle, whereas spherical aberration (c_4^0) decreased slightly toward the periphery. There was no correlation between defocus and angle, although some trends were found when the subjects were divided into groups depending on refractive error. When comparing results of different studies it has to be kept in mind that the coefficients differ depending on how the elliptical pupil is taken into consideration. © 2009 Optical Society of America

OCIS codes: 330.0330, 330.7325, 010.7350, 080.1010.

1. INTRODUCTION

During the past decades there has been a growing interest in the optical properties and the image quality on the retina of the human eye. Knowledge of the optical aberrations is important for understanding the function of the visual system and how it may be restored or even improved. Population studies have therefore been performed to investigate the image quality in normal eyes both foveally (on-axis) and peripherally (off-axis, in oblique viewing angles); some of the recent larger studies on on-axis aberrations can be found in [1–6], and the off-axis image quality has for example, been assessed in [7–17]. Today, most measurements of ocular aberrations are performed with the popular Hartmann–Shack (HS) method [18], and on-axis aberrations are classified and quantified with Zernike polynomials [19,20]. Because of their widespread use on-axis, the Zernike polynomials are beginning to be used also for describing wavefront aberrations in large off-axis angles; both in population studies (so far, in four smaller studies [7,8,10,14]) and in a technique to retrieve the optical properties of the inner eye through off-axis measurements [21,22]. But in oblique angles the pupil will appear elliptical in shape, and, since the Zernike polynomials are defined over a circular pupil, it is not straightforward how to present the off-axis wavefront aberrations; no standard exists, and the quantification can be made in different ways. Therefore, this paper fills two purposes: it is the first large study on the distribution of off-axis aberrations quantified with Zernike polynomials, and it discusses the effect of the elliptical pupil, using three alternative representations to present the results, including those representations used in previous studies. Additionally, MATLAB code is given in Appendix A to convert between the representations.

2. METHOD

The off-axis wavefront measurements were performed as part of a study on how to assess the peripheral refractive errors [12]. No cycloplegia was used, and the background illumination was kept low to have naturally large pupils. In total, 50 persons with normal, binocular vision were measured, but 7 of them had a pupil diameter smaller than 5 mm, and therefore only 43 subjects are presented in this paper (25 males and 18 females, ages 19 to 66 years, mean 31.5 years, and the central refractive errors were as follows: mean spherical equivalent, M, ranged from −7.50 D to 2.38 D, mean −1.27 D; the cross cylinder in 180°/90°, J0, ranged from −1.35 D to 0.50 D, mean −0.06 D; and the cross cylinder in 45°/135°, J45, ranged from −0.29 D to 0.35 D, mean −0.02 D). The right eye of each subject was measured at 0° (on-axis), 20°, and 30° off-axis in the horizontal nasal visual field (temporal retina).

The wavefront aberrations were measured with a laboratory HS sensor, which is described in detail in [23]. In short, a narrow beam of laser light (633 nm) was sent into the right eye in the desired measurement angle while the subject viewed fixation targets placed 3 m away with the left eye (except for the on-axis measurements when the target was aligned with the axis of the sensor and seen through lenses). A camera with an eye-tracker system was used to place the eye in the correct location and to confirm the off-axis angle. No spectacles or contact lenses

 © 2009 Optical Society of America

were used for the right eye and only the left eye, which viewed the fixation target, was corrected with the foveal prescription together with an additional +0.5 D to avoid accommodation. The pupil of the right eye was imaged on to the lenslet array (325 μm$\times$325 μm, focal length 18 mm) with a magnification of 0.85, and the resulting spot pattern was captured by a CCD camera. The shape of the pupil was estimated from the spot pattern by fitting an ellipse to the lenslets at the edge of the pupil. The wavefront was then reconstructed with Zernike polynomials over a circular aperture with a radius equal to the major radius of the elliptical pupil (this is the LC representation described below). Finally, the coefficients of three measurements were recalculated to the same pupil radius, adjusted for 550 nm wavelength, and averaged.

A. Quantification with Zernike Polynomials

When the pupil is elliptical, it has to be transformed into a circular aperture to enable quantification of the aberrations with Zernike polynomials. This circular aperture can be defined in three alternative ways, as can be seen in Fig. 1: LC, a large circular aperture encircling the elliptical pupil; SE, a circular aperture that is a stretched version of the elliptical pupil; and SC, a small circular aperture located within the elliptical pupil. The characteristics of each representation are described below. However, before going into the details, it should be emphasized that these versions all use the standard Zernike polynomials; it is only the shape of the pupil that is manipulated, which leads to a change in the values of the Zernike coefficients. The theory for converting between the coefficients for different apertures has previously been described in [24], but it did not include the MATLAB code for elliptical pupils, and for the reader's convenience that code is therefore given in Appendix A of this paper.

The procedure described in the section above corresponds to the first representation (LC) and has been used in some earlier studies [12,23]. Here the Zernike coefficients are calculated over a circular aperture that encircles all spots in the measurement image and describe a wavefront that is extrapolated outside the borders of the elliptical pupil (second image in Fig. 1). Together with information on the true elliptical shape of the pupil, they give a full description of the original wavefront and the peripheral image quality.

The second alternative (SE) stretches the elliptical pupil into a circular shape and has been used in earlier studies on peripheral wavefront aberrations expressed with Zernike coefficients [8,10,14,22]. Navarro *et al.* [14] used laser ray tracing with denser sampling along the minor axis of the pupil than along the major axis. The Zernike coefficients were then fitted to a stretched version of these sampling points, now spaced uniformly. Mathur *et al.* [8] and Atchison [10] measured the wavefront with a HS sensor and stretched the spot pattern into a circle before fitting Zernike coefficients. In this case, the stretching of the wavefront was performed so that the height of the wavefront was conserved (i.e., the slope of the wavefront was decreased). However, stretching has two drawbacks. First of all, a particular aberration will look different in the stretched version than in the original wavefront, which makes the interpretation of the Zernike coefficients less intuitive. This can be seen in Fig. 1: spherical aberration over an elliptical pupil will not be represented by rotationally symmetric coefficients in the stretching alternative (in this example the spherical aberration coefficient c_4^0 transforms into c_2^0, c_2^2, c_4^0, c_4^2, and c_4^4). The second drawback is that the amount of stretching (and hence the one-dimensional scaling of the Zernike coefficients) will change with the off-axis angle. This means that the stretching alternative is difficult to use if coefficients in different angels are to be compared.

The last representation (SC) is shown in the fourth image of Fig. 1. Here, only a circular part of the measured wavefront is used. The circular subaperture of the elliptical pupil can be realized by software that removes spots outside the circle in the measurement image by rescaling the extrapolated wavefront of the LC representation or by using a circular aperture placed in a plane conjugated with the pupil during the measurement. The aperture should be centered and its radius equal to, or smaller than, the minor axis of the elliptical pupil. This representation is less well correlated with the peripheral image quality in large oblique angles, because parts of the natural wavefront are omitted. However, it is convenient for investigation of optical changes with angle and has been used in [7,9,11,21,25].

B. Calculation of the Root-Mean-Square Error

Except for Zernike coefficients, another common way to quantify the amount of aberrations is the so-called root-mean-square (RMS) error. This is the standard deviation of the wavefront error over the pupil and can be calculated by taking the square of the height of the wavefront at each point, integrate, and divide by the area of the pu-

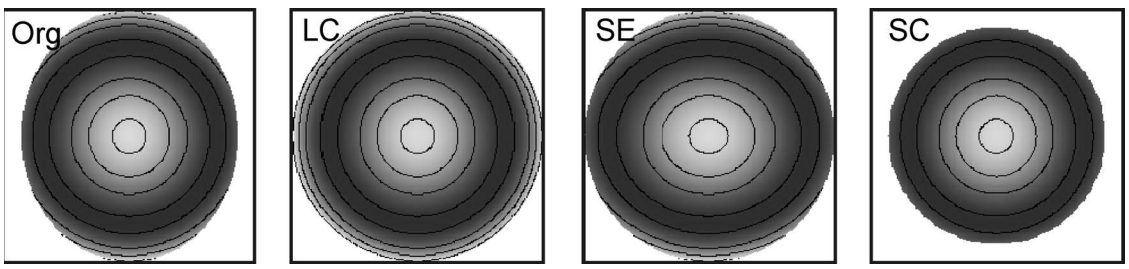

Fig. 1. A wavefront with spherical aberration and an elliptical pupil is converted into a circular aperture in three alternative ways: the leftmost image (Org) shows the original wavefront as it emerges from the eye; the second image (LC) presents the version that also contains extrapolated wavefront data; the third image (SE) is the alternative in which the original wavefront is stretched out into a circle; and the last image (SC) presents the version describing a circular subpart of the original wavefront.

pil. For wavefronts exiting circular pupils and expressed as Zernike coefficients, the RMS error takes a simple form; it equals the square root of the sum of the squares of the coefficients ($\sqrt{\Sigma c^2}$) [19,20]. Note that the piston and tilt of the wavefront should be removed before calculating the RMS.

With an elliptical pupil the RMS error can always be calculated from the height of the wavefront at each point as explained above. However, depending on how the wavefront is described with Zernike polynomials (the LC, SE, or SC representation), computing $\sqrt{\Sigma c^2}$ will give different values. The LC representation describes a larger wavefront than actually measured, and the coefficients will not predict the true RMS error since they include extrapolated parts; often they will give a value higher than the RMS error. Similarly, but in the opposite direction, the SC representation describes only a part of the actually measured wavefront. The SC coefficients will therefore predict a value that is often lower than the true RMS error. The SE representation, however, has the advantage that the RMS error is given directly by the Zernike coefficients. This is because the height of the wavefront and therefore the standard deviation of the wavefront error are preserved during the stretching. Note that the RMS values given in Table 2 below have all been calculated from the Zernike coefficients; i.e., it is only the SE columns that give the true RMS error over the complete elliptical pupil.

3. RESULTS

Table 1 gives statistics of the pupil shape and refractive errors of the right eye of the subjects in the three measured angles. The refractive errors were calculated from the wavefront by minimizing the RMS over a 4 mm circular pupil (SC representation) and are given as mean spherical equivalent ($M=-4\sqrt{3}\times c_2^{\,0}/r^2_{\text{pupil}}$), cross cylinder in 180°/90° ($\text{J0}=-2\sqrt{6}\times c_2^{\,2}/r^2_{\text{pupil}}$), and cross cylinder in 45°/135° ($\text{J45}=-2\sqrt{6}\times c_2^{\,-2}/r^2_{\text{pupil}}$); note that the values are calculated from the wavefront measurements also for the on-axis measurements. The eccentricity of the elliptical pupil was calculated as $\sqrt{(r^2_{\text{major}}-r^2_{\text{minor}})}/r_{\text{major}}$. On-axis the mean eccentricity was 0.26 (highest measured value was 0.50), in 20° off-axis the mean was 0.39 (max 0.64), and in 30° off-axis it was 0.53 (max 0.69). As a comparison, the cosine approximation, $r_{\text{minor}}=r_{\text{major}}\times\cos(\theta_{\text{off-axis}})$, would give 0, 0.34, and 0.50, respectively, corresponding to a minor axis equal to 100%, 94%, and 87% of the length of the major axis. As expected, the orientation of the elliptical pupil was random for the on-axis case and turned to horizontal for the off-axis measurements. The notation of the pupil axis is given according to the standard axis notation (the Tabo scheme); i.e., 180° means that the minor axis of the pupil is horizontal.

For the statistics on wavefront aberrations over the population in terms of Zernike coefficients, we used the previously mentioned representations (notation following the ANSI standard [19]): LC, circular pupil with a diameter of 5 mm that is extrapolated for some persons in 20° and 30° off-axis (many subjects had a minor pupil diameter larger than 5 mm and therefore no true extrapolation); SE, elliptical pupil with a major diameter of 5 mm and a minor diameter that follows the cosine approximation and is oriented along the 180° meridian of the eye; and SC, circular pupil with a diameter of 4 mm, which is not extrapolated for any of the subjects. Table 2 gives the absolute values of the individual Zernike coefficients for these three representations, averaged over the 43 subjects in 0°, 20°, and 30° off-axis in the horizontal nasal visual field of the right eye (the on-axis aberrations are given with representation LC and SC only). Note that the statistics given in Table 2 was performed on the unsigned coefficients to give a better estimate of the contribution of each aberration to the wavefront variance; the same type of calculations were also made on the signed third- and fourth-order coefficients for the SC representation and are presented in Fig. 2 for comparison.

These changes with angle for the signed Zernike coefficients are further illustrated in Table 3 as correlation coefficients for the two representations with unstretched pupil (SC and LC). For the refractive errors, the horizontal viewing angle induced astigmatism with an axis of approximately 90° (negative cylinder); $c_2^{\,2}$ showed a high correlation with the angle (almost 0.8). No correlation between defocus and the angle was found. Generally, the high-order aberrations increased significantly with the angle; from a RMS error of 0.11 to 0.28 μm over the 4 mm pupil (correlation coefficient of 0.6). The high-order aberration coefficient with highest correlation (−0.73) was horizontal coma ($c_3^{\,1}$), but also horizontal trefoil ($c_3^{\,3}$), quadrifoil ($c_4^{\,-4}$), and secondary astigmatism ($c_4^{\,2}$) got more pronounced with the angle, whereas vertical trefoil ($c_3^{\,-3}$) and spherical aberration ($c_4^{\,0}$) showed a trend toward less aberration in the periphery. In Fig. 3 the angular variation of the two coefficients with largest correlation ($c_2^{\,2}$ and $c_3^{\,1}$) are shown for both the SC and the LC representations. As can be seen, astigmatism increases in the expected quadratic behavior, whereas coma shows a more linear progression [26].

Table 1. Population Statistics of the 43 Subjects in the Study (Mean Value±Standard Deviation)

Parameter	0°	20°	30°
Major pupil diameter (mm)	6.5±0.8	6.4±0.8	6.4±0.8
Pupil eccentricity	0.26±0.09	0.39±0.09	0.53±0.08
Orientation of minor pupil axis (degrees)	Random	2±16	2±7
Spectacle refraction, M (diopters)	−1.33±1.66	−1.65±1.60	−1.25±1.59
Spectacle refraction, J0 (diopters)	−0.01±0.37	−0.72±0.40	−1.37±0.51
Spectacle refraction, J45 (diopters)	−0.03±0.17	0.07±0.21	0.12±0.27

Table 2. Variation with Off-Axis Angle (0°, 20°, and 30°) for the Absolute Values of Zernike Coefficients over the Population for Three Different Pupil Shapes[a]

	0°		20°			30°		
Zernike Coefficient	LC: Large Circle, 5 mm	SC: Small Circle, 4 mm	LC: Large Circle, 5 mm	SE: Stretched Ellipse, 5 mm	SC: Small Circle, 4 mm	LC: Large Circle, 5 mm	SE: Stretched Ellipse, 5 mm	SC: Small Circle, 4 mm
c_2^{-2}	0.161±0.144	0.103±0.091	0.205±0.188	0.193±0.176	0.131±0.117	0.286±0.253	0.250±0.219	0.185±0.157
c_2^{0}	1.501±1.230	0.929±0.799	1.731±1.208	1.602±1.129	1.077±0.771	1.412±1.173	1.138±1.025	0.885±0.755
c_2^{2}	0.315±0.338	0.205±0.217	0.931±0.506	0.743±0.540	0.591±0.328	1.739±0.660	1.314±0.694	1.122±0.417
c_3^{-3}	0.083±0.051	0.050±0.031	0.069±0.053	0.065±0.050	0.038±0.031	0.071±0.055	0.060±0.050	0.038±0.031
c_3^{-1}	0.073±0.058	0.040±0.033	0.075±0.053	0.073±0.053	0.042±0.032	0.077±0.056	0.071±0.053	0.038±0.030
c_3^{1}	0.061±0.056	0.035±0.029	0.271±0.171	0.239±0.148	0.154±0.088	0.467±0.253	0.337±0.186	0.253±0.134
c_3^{3}	0.053±0.041	0.032±0.023	0.066±0.057	0.061±0.055	0.037±0.033	0.097±0.076	0.074±0.066	0.057±0.046
c_4^{-4}	0.016±0.013	0.010±0.008	0.024±0.019	0.022±0.017	0.014±0.010	0.034±0.025	0.027±0.021	0.018±0.013
c_4^{-2}	0.015±0.011	0.009±0.006	0.016±0.012	0.014±0.012	0.009±0.007	0.019±0.016	0.015±0.013	0.010±0.009
c_4^{0}	0.069±0.054	0.033±0.026	0.062±0.050	0.055±0.045	0.028±0.021	0.051±0.056	0.038±0.032	0.023±0.018
c_4^{2}	0.022±0.013	0.010±0.007	0.026±0.020	0.026±0.018	0.015±0.012	0.043±0.043	0.037±0.030	0.023±0.018
c_4^{4}	0.020±0.017	0.012±0.010	0.024±0.019	0.024±0.018	0.014±0.011	0.034±0.027	0.026±0.016	0.017±0.015
RMS 5th ord	0.033±0.013	0.018±0.008	0.041±0.015	0.036±0.013	0.022±0.009	0.059±0.049	0.039±0.013	0.027±0.011
RMS 6th ord	0.020±0.011	0.007±0.004	0.025±0.012	0.022±0.011	0.010±0.006	0.041±0.032	0.026±0.012	0.013±0.006
RMS 7th ord	0.012±0.006	0.004±0.003	0.017±0.009	0.015±0.008	0.006±0.004	0.029±0.033	0.017±0.010	0.009±0.005
RMS 8th ord	0.004±0.003	0.001±0.001	0.007±0.008	0.005±0.006	0.001±0.001	0.012±0.015	0.006±0.007	0.002±0.002
RMS 3rd–9th ord	0.190±0.072	0.105±0.040	0.339±0.156	0.304±0.135	0.188±0.081	0.524±0.253	0.388±0.177	0.281±0.129

[a]Large circular aperture of 5 mm in diameter (LC), elliptical aperture stretched into a circle of 5 mm (SE), and small circular aperture of 4 mm (SC) (mean value ± standard deviation in μm over the population).

4. DISCUSSION

The HS principle can be used to measure central as well as peripheral wavefronts when modified to handle large aberrations and elliptical pupils. One of the remaining obstacles is how to quantify the peripheral aberrations. In this study we used Zernike polynomials and suggested three alternative ways to describe the aberrated wavefront over an elliptical pupil. It should be stressed that Zernike polynomials are not the optimum functions for describing wavefronts with an elliptical outline. Nor are the three alternatives described here the only ways to manipulate the pupil, but they are used in practice within visual optics research today.

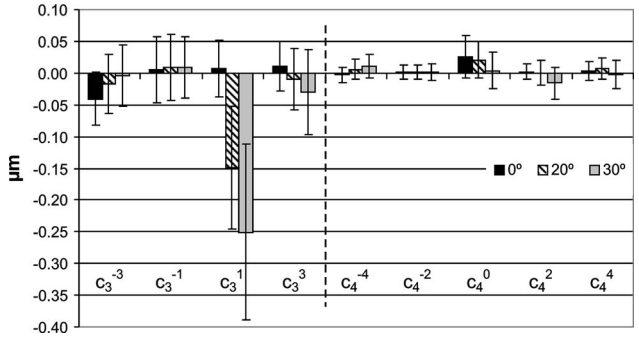

Fig. 2. Signed third- and fourth-order Zernike coefficients for a 4 mm circular subpupil (SC) in the three measured angles. The rectangular bars are the mean values, and the error bars show the standard deviation over the population.

Table 3. Correlation with Off-Axis Angle for Each Signed Zernike Coefficient in μm over a 5 mm Circular Aperture (LC) and a 4 mm Circular Aperture (SC)[a]

Zernike Coefficient	Correlation with Angle (signed LC)	Correlation with Angle (signed SC)
c_2^{-2}	−0.270*	−0.271*
c_2^{0}	−0.010	−0.001
c_2^{2}	0.780*	0.783*
c_3^{-3}	0.265*	0.315*
c_3^{-1}	−0.031	0.031
c_3^{1}	−0.727*	−0.727*
c_3^{3}	−0.268*	−0.298*
c_4^{-4}	0.306*	0.348*
c_4^{-2}	−0.021	0.002
c_4^{0}	−0.114	−0.260*
c_4^{2}	−0.122	−0.318*
c_4^{4}	0.030	−0.104
RMS 5th ord	0.313*	0.382*
RMS 6th ord	0.362*	0.394*
RMS 7th ord	0.300*	0.412*
RMS 8th ord	0.324*	0.324*
RMS 3rd–9th ord	0.598*	0.609*

[a]Pearson correlation coefficients, $p < 0.05$ are marked with *.

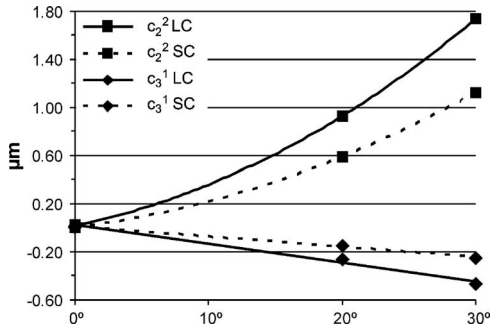

Fig. 3. Variation with angle for horizontal astigmatism (c_2^2, squares) and coma (c_3^1, diamonds) for two circular pupil sizes: 5 mm (LC, solid curves) and 4 mm (SC, dashed curves). The averages of the two signed Zernike coefficients are plotted in micrometers for the horizontal off-axis angles of 0°, 20°, and 30°. The curves are best-fit curves: c_2^2 follows a quadratic trend, for LC $0.0012\times\theta^2_{\text{off-axis}}+0.022\times\theta_{\text{off-axis}}$ and for SC $0.0008\times\theta^2_{\text{off-axis}}+0.013\times\theta_{\text{off-axis}}$, whereas c_3^1 has a more linear behavior, for LC −0.016 μm/deg and for SC −0.0085 μm/deg.

There are advantages and disadvantages with all three alternatives. The SC representation, with a smaller aperture confined within the elliptical pupil, neglects parts of the wavefront, but it has the advantage that the coefficients can be treated in the same manner as for foveal measurements. An additional advantage with SC, as well as with the LC alternative, is that they can be directly used to compare the coefficients between different viewing angles. The coefficients with the SC and the LC representation are closely related; the SC coefficients can be easily obtained by scaling down the large pupil of the LC representation to the SC size in the same manner as when changing the pupil size for on-axis measurements [27]. The LC and the SE representations both give a full description of the wavefront, but they require extra manipulation to calculate the retinal image quality.

An example of what might happen with the point-spread function (PSF) if the representations are used incorrectly is shown in Fig. 4 for a wavefront with spherical aberration exiting an elliptical pupil. The true PSFs are given in the leftmost column (the upper is for a 30° off-angle and the lower for 50°). The middle column illustrates the effect of using the LC representation without removing the extrapolated part of the wavefront, i.e., calculating the PSF directly from the extrapolated wavefront over the circular aperture with the same diameter as the major axis of the elliptic pupil. The rightmost column shows the PSFs if the SE representation is used without taking the stretched coordinate system into consideration, i.e., calculating the PSF directly from the stretched wavefront over the circular aperture with the same diameter as the major axis of the elliptic pupil. If results of different studies are compared, it is important to keep in mind that the Zernike coefficients for the different representations differ, just as the coefficients for circular pupils differ depending on pupil size; in 30° off-axis, for example, the RMS of the high-order aberrations with alternative SE is 74% of that of alternative LC, and alternative SC is only 54% of LC. Additionally, the three representations will give slightly different trends when the coefficients in different off-axis angles are compared.

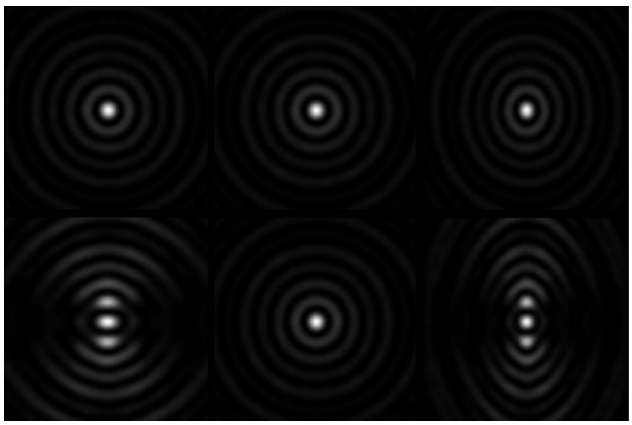

Fig. 4. Effect on the PSF if the Zernike representations are used incorrectly. The figures show pure spherical aberration for an elliptical pupil; on the upper row the off-angle is 30°, and on the lower row the angle is 50°. The leftmost column shows the true PSFs, the middle column illustrates the effect of using the LC representation without removing the extrapolated part of the wavefront, and in the rightmost column the SE representation is used without taking the stretched coordinate system into consideration.

The on-axis results presented here are in good agreement with earlier population studies. For example, the overview by Salmon and van de Pol [1] gives the following mean values and standard deviations in micrometers for a 5 mm circular pupil (the data of the current study in parentheses): high-order RMS 0.186±0.078 (0.190±0.072), and the three largest aberrations are vertical trefoil c_3^{-3} 0.069±0.056 (0.083±0.051), vertical coma c_3^{-1} 0.082±0.069 (0.073±0.058), and spherical aberration c_4^0 0.064±0.049 (0.069±0.054). Also off-axis we found trends similar to those of earlier studies (see e.g., the review [28]). One reason why no general change with off-axis angle was found for defocus is that subjects of different refractive states were averaged. If the group is divided into emmetropes [abs(M)=0.5 D, 13 persons], hyperopes ($M>-0.5$ D, 11 persons), and myopes ($M<-0.5$ D, 19 persons) the trend becomes clearer: the emmetropic group was on average 0.11 D more myopic in 30° off-axis compared with the foveal refraction (M calculated from the c_2^0 of the SC method); the hyperopes were even more myopic, 0.56 D relative to the fovea; whereas the myopes showed the opposite trend and had relative hyperopia of 0.59 D in 30° off-axis. These trends have also been noted in earlier studies, and the relative peripheral hyperopia of myopic eyes is especially of interest for myopia research [28]. Astigmatism increased in a quadratic manner in all subjects, as expected from the predictions of the Seidel theory [26]. Additionally, the Seidel theory and all studies [7,8,10,14], including the present, show a linear increase in coma with angle. The increase of 0.007 μm/deg in c_3^1 for the 4 mm SC representation is close to the 0.008 μm/deg from the study by Lundström *et al.* [7]. The 0.02–0.03 μm/deg reported by Atchison [10] for c_3^1 over a 6 mm SE aperture, which scales down to 0.012–0.017 μm/deg for a 5 mm pupil, is also in reasonably good agreement with the 0.009 μm/deg found here for the SE representation. Additionally, Atchison found a slight decrease in spherical aberration with angle in most subjects, which is also visible in all three representations

of the Zernike coefficient c_4^0 of this study. Regarding the high-order RMS error, Navarro [14] used the SE representation and found a close to linear increase with angle with the RMS in 40° off-axis being double the foveal value, whereas Lundström *et al.* [7] using SC representation found an even stronger and more quadratic increase with almost three times the foveal value in 30° off-axis on the temporal retina. The corresponding values in this study were 2 and 2.7 times for the SE and SC methods, respectively, and although both methods showed a quadratic increase in RMS, it was more pronounced for the SC alternative.

5. CONCLUSION

This paper presents a population study of peripheral wavefront aberrations in terms of Zernike coefficients. The aberrations in 0°, 20°, and 30° off-axis in the horizontal nasal visual field of the right eye for 43 normal subjects are represented with Zernike coefficients in three alternative ways; MATLAB conversion code is given in Appendix A. All three representations show similar trends: astigmatism and coma increase strongly with off-axis angle in a quadratic and linear manner, respectively, whereas spherical aberration decreases slightly. The mean spherical equivalent does not correlate with angle, although some trends can be seen when emmetropes, hyperopes, and myopes are analyzed separately.

APPENDIX A: MATLAB CODE FOR CONVERTING BETWEEN ZERNIKE COEFFICIENTS IN THE STRETCHED AND NONSTRETCHED FORM

This code converts between the Zernike representations LC (circular aperture with extrapolated wavefront) and SE (elliptical pupil stretched into a circle), to get the SC alternative (circular aperture within the pupil) simply scale down the coefficients of LC. The program returns the stretched or destretched Zernike coefficients, C2, from the original set, C1, both in standard order. etaE=minor pupilaxis/major pupilaxis to strech the elliptical pupil, major/minor to destretch. thetaE=angle in radians measured from the horizontal coordinate axis to the minor pupilaxis in counterclockwise direction. For more details see [24].

```
function C2=TransformCellipsPub(C1,etaE,thetaE)

jnm=length(C1)-1; nmax=ceil((-3+sqrt(9+8*jnm))/2);
jmax=nmax*(nmax+3)/2;
S=zeros(jmax+1,1); S(1:length(C1))=C1; C1=S;
clear S
P=zeros(jmax+1); N=zeros(jmax+1); R=zeros(jmax+1);
CC1=zeros(jmax+1,1); counter=1;
for m=-nmax:nmax
for n=abs(m):2:nmax
jnm=(m+n*(n+2))/2;
P(counter,jnm+1)=1;
N(counter,counter)=sqrt(n+1);
for s=0:(n-abs(m))/2
R(counter-s,counter)=(-1)^s*factorial(n
-s)/(factorial(s)*factorial((n+m)/2-s)*factorial((n-m)/2-s));
end
if m<0, CC1(jnm+1)=(C1((-m+n*(n+2))/2+1)
+i*C1(jnm+1))sqrt(2);
elseif m==0, CC1(jnm+1)=C1(jnm+1);
else, CC1(jnm+1)=(C1(jnm+1)-i*C1((-m+n*(n+2))/2
+1))/sqrt(2); end
counter=counter+1;
end, end

ETAE=[ ];
for m=-nmax:nmax
for n=abs(m):2:nmax
ETAE=[ETAEP*(transformE(n,m,jmax,,etaE,thetaE))];
end, end
C=inv(P)*inv(N)*inv(R)*ETAE*R*N*P;
CC2=C*CC1;

C2=zeros(jmax+1,1);
for m=-nmax:nmax
for n=abs(m):2:nmax
jnm=(m+n*(n+2))/2;
if m<0, C2(jnm+1)=imag(CC2(jnm+1)
-CC2((-m+n*(n+2))/2+1))/sqrt(2);
elseif m==0,
C2(jnm+1)=real(CC2(jnm+1));
else,
C2(jnm+1)=real(CC2(jnm+1)+CC2((-m+n*(n+2))/2
+1))/sqrt(2);
end, end, end

function Eta=transformE(n,m,jmax,etaE,thetaE)
Eta=zeros(jmax+1,1);
for p=0:((n+m)/2)
for q=0:((n-m)/2);
mnew=n; mnew=m-2*p+2*q; jnm=(mnew
+nnew*(nnew+2))/2;
Eta(floor(jnm+1))=Eta(floor(jnm+1))+0.5^n*nchoosek((n
+m)/2,p)*nchoosek((n-m)/2,q)*(etaE+1)^(n-p-q)*(etaE
-1)^(p+q)*exp(i*2*(p-q)*thetaE);
end, end
```

ACKNOWLEDGMENTS

The authors are very grateful to all the volunteering subjects. The financial support for this research was provided by the European Marie Curie research training network MY EUROPIA (MRTN-CT-2006-034021), the Carl Trygger Foundation, the Göran Gustafsson Foundation, and the Carl-Johan and Berit Wettergren Foundation.

REFERENCES

1. T. Salmon and C. van de Pol, "Normal-eye Zernike coefficients and root-mean-square wavefront errors," J. Cataract Refractive Surg. **32**, 2064–2074 (2006).
2. H. Cheng, J. K. Barnett, A. S. Vilupuru, J. D. Marsack, S. Kasthurirangan, R. A. Applegate, and A. Roorda, "A population study on changes in wave aberrations with accommodation," J. Vision **4**, 272–280 (2004).
3. L. Wang and D. D. Koch, "Ocular higher-order aberrations in individuals screened for refractive surgery," J. Cataract Refractive Surg. **29**, 1896–1903 (2003).

4. J. F. Castejón-Mochón, N. López-Gil, A. Benito, and P. Artal, "Ocular wave-front aberration statistics in a normal young population," Vision Res. **42**, 1611–1617 (2002).
5. L. N. Thibos, X. Hong, A. Bradley, and X. Cheng, "Statistical variation of aberration structure and image quality in a normal population of healthy eyes," J. Opt. Soc. Am. A **19**, 2329–2348 (2002).
6. J. Porter, A. Guirao, I. G. Cox, and D. R. Williams, "Monochromatic aberrations of the human eye in a large population," J. Opt. Soc. Am. A **18**, 1793–1803 (2001).
7. L. Lundström, A. Mira-Agudelo, and P. Artal, "Peripheral optical errors and their change with accommodation differ between emmetropic and myopic eyes," J. Vision **9**, 17 (2009).
8. A. Mathur, D. A. Atchison, and D. H. Scott, "Ocular aberrations in the peripheral visual field," Opt. Lett. **33**, 863–865 (2008).
9. M. T. Sheehan, A. V. Goncharov, V. M. O′Dwyer, V. Toal, and C. Dainty, "Population study of the variation in monochromatic aberrations of the normal human eye over the central visual field," Opt. Express **15**, 7367–7380 (2007).
10. D. A. Atchison, "Higher order aberrations across the horizontal visual field," J. Biomed. Opt. **11**, 034026 (2006).
11. D. A. Atchison, S. D. Lucas, R. Ashman, M. A. Huynh, D. W. Schilt, and P. Q. Ngo, "Refraction and aberration across the horizontal central 10 degrees of the visual field," Optom. Vision Sci. **83**, 213–21 (2006).
12. L. Lundström, J. Gustafsson, I. Svensson, and P. Unsbo, "Assessment of objective and subjective eccentric refraction," Optom. Vision Sci. **82**, 298–306 (2005).
13. A. Guirao and P. Artal, "Off-axis monochromatic aberrations estimated from double pass measurements in the human eye," Vision Res. **39**, 207–217 (1999).
14. R. Navarro, E. Moreno, and C. Dorronsoro, "Monochromatic aberrations and point-spread functions of the human eye across the visual field," J. Opt. Soc. Am. A **15**, 2522–2529 (1998).
15. R. Navarro, P. Artal, and D. R. Williams, "Modulation transfer of the human eye as a function of retinal eccentricity," J. Opt. Soc. Am. A **10**, 201–212 (1993).
16. J. A. M. Jennings and W. N. Charman, "Off-axis image quality in the human eye," Vision Res. **21**, 445–455 (1981).
17. J. A. M. Jennings and W. N. Charman, "Optical image quality in the peripheral retina," Am. J. Optom. Physiol. Opt. **55**, 582–590 (1978).
18. J. Liang, B. Grimm, S. Goelz, and J. F. Bille, "Objective measurement of wave aberrations of the human eye with use of a Hartmann-Shack wave-front sensor," J. Opt. Soc. Am. A **11**, 1949–1957 (1994).
19. American National Standards Institute, "Methods for reporting optical aberrations of eyes," ANSI Z80.28–2004 (2004).
20. L. N. Thibos, R. A. Applegate, J. T. Schwiegerling, R. Webb, and VSIA Standards Taskforce Members, "Standards for reporting the optical aberrations of eyes," J. Refract. Surg. **18**, 652–660 (2002).
21. A. V. Goncharov, M. Nowakowski, M. T. Sheehan, and C. Dainty, "Reconstruction of the optical system of the human eye with reverse ray-tracing," Opt. Express **16**, 1692–1703 (2008).
22. X. Wei and L. Thibos, "Modeling the eye's optical system by ocular wavefront tomography," Opt. Express **16**, 20490–20502 (2008).
23. L. Lundström, P. Unsbo, and J. Gustafsson, "Off-axis wave front measurements for optical correction in eccentric viewing," J. Biomed. Opt. **10**, 034002 (2005).
24. L. Lundström and P. Unsbo, "Transformation of Zernike coefficients: scaled, translated, and rotated wavefronts with circular and elliptical pupils," J. Opt. Soc. Am. A **24**, 569–577 (2007).
25. L. Lundström, S. Manzanera, P. M. Prieto, D. B. Ayala, N. Gorceix, J. Gustafsson, P. Unsbo, and P. Artal, "Effect of optical correction and remaining aberrations on peripheral resolution acuity in the human eye," Opt. Express **15**, 12654–12661 (2007).
26. M. Born and E. Wolf, *Principles of Optics*, 7th ed. (Cambridge Univ. Press, 1999), Chap. 5.
27. J. Schwiegerling, "Scaling Zernike expansion coefficients to different pupil sizes," J. Opt. Soc. Am. A **19**, 1937–1945 (2002).
28. W. N. Charman, "Aberrations and myopia," Ophthalmic Physiol. Opt. **25**, 285–301 (2005).